Fabrication of cationic cellulose nanofibrils/sodium alginate beads for Congo red removal

Wu, Meiyan; Zhang, Yidong; Feng, Xiaoyan; Yan, Fei; Li, Qian; Cui, Qiu; Li, Bin

Published in:
iScience

DOI:
10.1016/j.isci.2023.107783

Published: 20/10/2023

Document Version
Final published version

Document License
CC BY-NC-ND

iScience

CellPress
OPEN ACCESS

Article

Fabrication of cationic cellulose nanofibrils/sodium alginate beads for Congo red removal

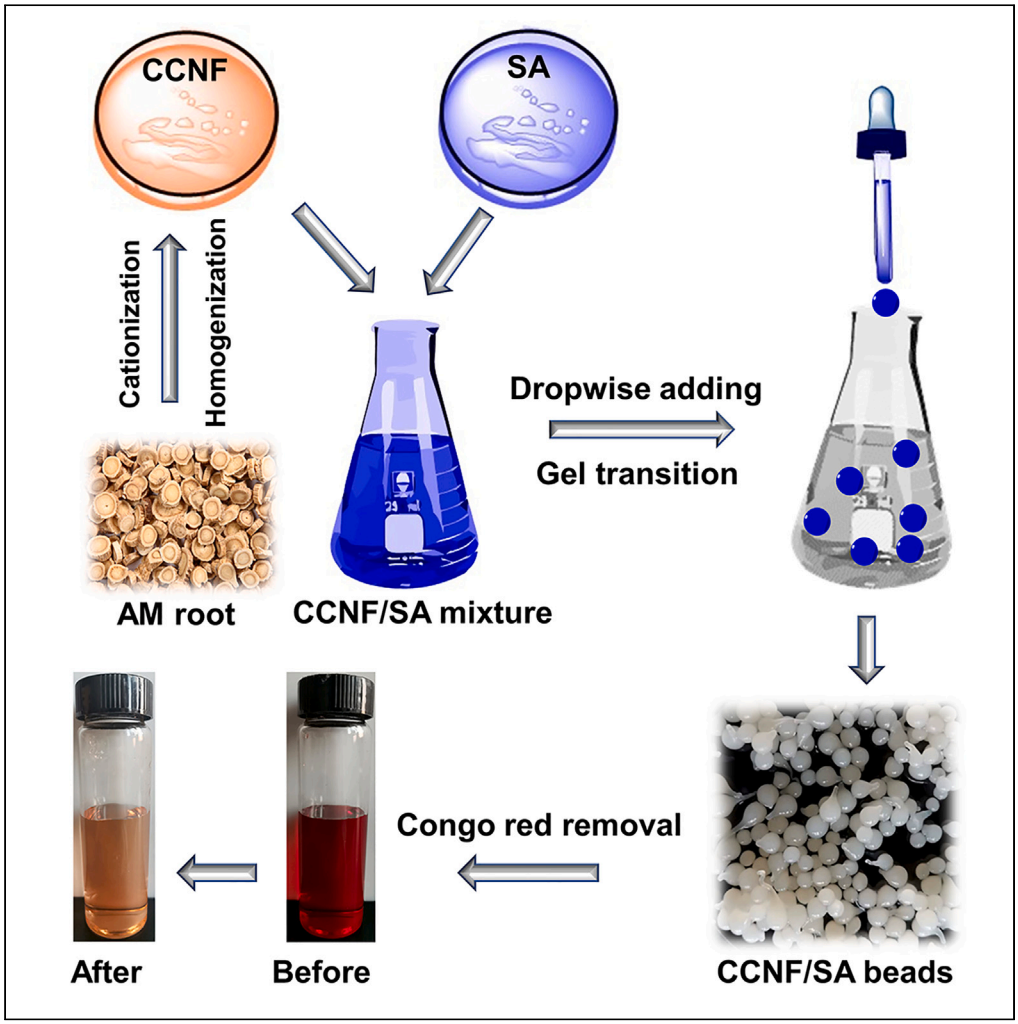

Meiyan Wu, Yidong Zhang, Xiaoyan Feng, Fei Yan, Qian Li, Qiu Cui, Bin Li

qianli@sdu.edu.cn (Q.L.)
libin@qibebt.ac.cn (B.L.)

Highlights

CCNF from Chinese herb residues was crosslinked with SA to prepare CCNF/SA beads

The beads with porous internal structure were beneficial to adsorption of Congo red

Hydrogen bond and electrostatic adsorption were the dominant adsorption mechanism

The beads could be effectively reused for the treatment of Congo red wastewater

Wu et al., iScience 26, 107783
October 20, 2023
https://doi.org/10.1016/j.isci.2023.107783

iScience

CellPress
OPEN ACCESS

Article

Fabrication of cationic cellulose nanofibrils/sodium alginate beads for Congo red removal

Meiyan Wu,[1] Yidong Zhang,[1,2] Xiaoyan Feng,[1] Fei Yan,[1] Qian Li,[3,*] Qiu Cui,[1,4,5] and Bin Li[1,4,5,6,*]

SUMMARY

Congo red is hard to remove from dye wastewater due to its structure stability and high chemical oxygen demand. In this study, cationic cellulose nanofibrils (CCNF) prepared from herb residues was physically crosslinked with sodium alginate (SA) in the presence of calcium ions, and the obtained CCNF/SA beads were used to adsorb Congo red. Results showed that CCNF/SA beads with porous internal structure were beneficial to adsorption. The maximum adsorption capacity of Congo red could reach to 518.4 mg/g, which was superior to most cellulose-based adsorption materials. Furthermore, the equilibrium adsorption isotherms and XPS analysis indicated the adsorption for Congo red was a physical process, and hydrogen bond and electrostatic adsorption were proposed as dominant adsorption mechanism. In addition, the Congo red removal efficiency of the beads was still higher than 70% after three cycles. Therefore, this high efficiency and green beads have great potential as adsorbents for anionic dyes removal.

INTRODUCTION

With the rapid development of textile industry, the discharge of dye wastewater becomes a severe threat to aquatic environment; dyes and their degradation products also cause allergies, skin irritation, and poisoning to human beings. The commonly used Congo red is one of toxic anionic dyes, and the wastewater containing Congo red with molecular size of 2.6 nm is not easy to treat due to its high colority, difficulty of degradation, high chemical oxygen demand, and strong toxicity. To solve this problem, many chemical, biological, and physical methods for Congo red removal were studied. Among them, physical adsorption method was widely used thanks to the advantages of convenient operation, high-efficiency, and eco-friendly, and many corresponding adsorbents were developed, such as boehmite microspheres,[1] zeolites,[2] activated carbon, metal-organic framework,[3,4] supramolecular gelator,[5] etc. However, these adsorbents usually involved expensive or hazardous chemicals, and complex preparation and separation method. Therefore, it is still a challenge to fabricate a green and stable adsorbent with low price and simple preparation method for Congo red removal.

Recently, natural polymers, such as cellulose, alginate, and chitosan, were widely reported to prepare adsorbents for Congo red removal.[6,7] In particular, cationic cellulose nanofibrils (CCNF) as cellulose derivatives exhibited an amazing adsorption selectivity and high adsorption capacity for anionic Congo red due to the large surface area and high cationic charge density.[8,9] Furthermore, CCNF could be prepared using pulp or agricultural residues, which largely decreased the material cost. *Astragalus membranaceus* (AM) as a traditional Chinese medicine is widely planted in Southeast Asia, Europe, and North America.[10] After extraction of active substances in pharmaceutical factory, the AM residues (AM-R) as solid waste have not been well utilized, resulting in the waste of resources. As known, AM-R was rich in cellulose and could be used to prepare CCNF hydrogels for the application of handy skin wound dressing.[11] Nevertheless, this CCNF from AM-R failed to directly prepare the adsorbent due to the poor stability in wastewater. Here, sodium alginate (SA) as a natural polymer has abundant hydroxyl and carboxyl groups, which can occur gelation with the presence of calcium ions to obtain stable and regular gel materials.[12] A previous report showed that chitosan/SA hydrogel could adsorb heavy metal ions because of the chelate effect of SA and chitosan.[13] In addition, SA as an anionic polyelectrolyte could also be physically crosslinked with cationic CCNF to prepare gel materials with good mechanical properties. Thus, it has great potential to obtain low-priced CCNF/SA composite for Congo red adsorption.

Therefore, in this work, the CCNF were first prepared using the AM-R, and the CCNF/SA beads were obtained through adding the mixture of CCNF and SA into $CaCl_2$ solution. Then, the lyophilized CCNF/SA beads were used for Congo red removal test. The technical route of this

[1]CAS Key Laboratory of Biofuels, Qingdao Institute of Bioenergy and Bioprocess Technology, Chinese Academy of Sciences, Qingdao 266101, P.R. China
[2]Laboratory of Natural Materials Technology, Åbo Akademi University, 20500 Turku, Finland
[3]Shandong Provincial Key Laboratory of Water Pollution Control and Resource Reuse, Shandong Key Laboratory of Environmental Processes and Health, School of Environmental Science and Engineering, Shandong University, Qingdao 266237, P.R. China
[4]Shandong Energy Institute, Qingdao 266101, P.R. China
[5]Qingdao New Energy Shandong Laboratory, Qingdao 266101, P.R. China
[6]Lead contact
*Correspondence: qianli@sdu.edu.cn (Q.L.), libin@qibebt.ac.cn (B.L.)
https://doi.org/10.1016/j.isci.2023.107783

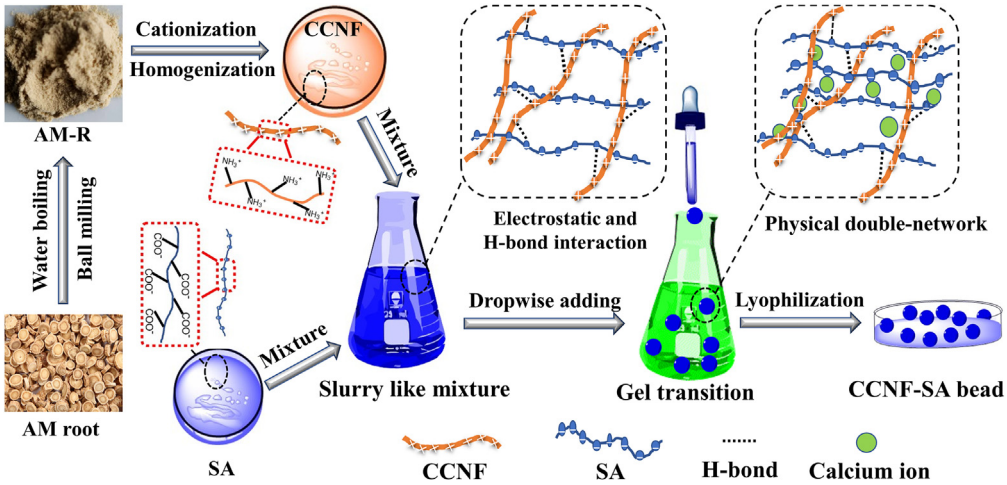

Figure 1. The technical route of this work.

experiment is shown in Figure 1. Comprehensive characterization showed that the obtained CCNF/SA beads exhibited low swelling ratio and high adsorption capacity for Congo red, and the adsorption curves were well fitted by Langmuir and Freundlich models. In addition, the adsorption kinetics of the CCNF/SA beads was also investigated. This work provides a new and green approach for the high value-added application of herb residues, and has a broad prospect to further develop the cellulose-based materials for dye adsorption.

RESULTS AND DISCUSSION

Chemical structure of raw material

According to the component analysis of AM and AM-R (Table 1), the main ingredients in AM were glucan, extractives, hemicellulose (xylan and arabinan), lignin, and ash, and the relative content of glucan (cellulose, 47.3 $\pm$ 4.8%) of AM-R was significantly increased 58.2%, after removing part of active ingredients (extractives) and ash through water boiling (i.e., hydrothermal treatment).[14] Therefore, AM-R as a cellulose-rich raw material was appropriate to prepare cellulose nanofibrils.

Moreover, the chemical structure of AM and AM-R was investigated using Fourier transform infrared (FTIR) spectra (Figure 2A). The peaks at 2919 and 1748 cm^{-1} belonged to the stretching vibration of C–H and C=O in cellulose.[11] Simultaneously, the peaks at 1646 and 1055 cm^{-1} assigned to the adsorbed moisture and C–H vibration of the pyranoid ring.[15] However, the broad peak at 3391 cm^{-1} in the spectrum of AM shifted to 3432 cm^{-1} in the spectrum of AM-R. After zoomed in (3750–3000 cm^{-1}), the H-bond and O–H bond could be evaluated on the basis of the peak-differentiating and imitating method. As shown in Figures 2B and 2C, the fit peaks around 3535 cm^{-1} were attributed to the O–H bond, and the fit peaks around 3326 cm^{-1} were related to H-bond in all spectra.[15] Compared with the fit peaks of AM, the intensity of O–H bond decreased and the intensity of the corresponding H-bond increased in AM-R. These results were because of the increased content of cellulose in AM-R, thus enhancing the intermolecular H-bond interaction after extraction of active ingredients from AM.

In addition, the crystalline structure of AM and AM-R was further investigated using X-ray diffraction. As can be seen from Figure 2D, the pattern of AM was similar with AM-R, and the main characteristic diffraction peaks at 16.5°, 22.6°, and 34.4° indicated that the cellulose I structure had no change after boiling.[16]

Characterization of CCNF/SA beads

After alkalization and etherification, the yield of CCNF was 67.1% based on the amount of AM-R. The zeta potential of 0.01 wt. % CCNF suspension was 54.8 $\pm$ 2.9 mV (Table 2), and the degree of substitution of CCNF was 0.15 $\pm$ 0.02, indicating the cationic characterization of CCNF. Moreover, as can be seen from Figure 3A, the diameter of CCNF was 25.6 $\pm$ 2.1 nm, and the CCNF was aggregated after adding SA with the mass ratio of 40:1 (CCNF suspension (concentration 0.65 wt. %): SA powder). Specially, when the mass ratio of CCNF suspension to SA powder was increased to 50:1 or 60:1, the homogeneously dispersed CCNF could be observed in transmission electron microscopy images. This phenomenon was due to the electrostatic interaction between the positively charged CCNF and the negatively charged SA.[11] After adding the mixture of CCNF and SA to $CaCl_2$ solution dropwise, the gelation between SA and calcium ion occurred and calcium alginate beads embraced with CCNF (CCNF/SA beads) quickly formed. As shown in Figure 3B, pure calcium alginate beads were regular and transparent, while the formed CCNF/SA beads with the mass ratio of 40:1 exhibited long tails, and the CCNF/SA beads with the mass ratios of 50:1 and 60:1 were relatively regular shaped. Herein, when the mass ratio of CCNF suspension to SA was lower than 40:1, high viscosity of mixture led to the formation of long tails on beads, and when the mass ratio of CCNF suspension to SA was higher than 60:1, the mixture failed to form regular gel balls due to the low content of SA in $CaCl_2$ solution. Therefore, the CCNF/SA beads with the mass ratios of 40:1, 50:1, and 60:1 were studied in the following work, and the bead samples were correspondingly named as the 40:1 beads, the 50:1 beads, and the 60:1 beads.

Table 1. Chemical compositions of AM and AM-R

Ingredients	AM	AM-R
Glucan (%)	29.9 ± 5.4	47.3 ± 4.8
Xylan (%)	2.8 ± 0.4	4.5 ± 0.3
Arabinan (%)	2.5 ± 0.3	4.4 ± 0.2
Lignin (%)	3.4 ± 0.1	5.9 ± 0.4
Extractives (%)	47.3 ± 1.5	16.7 ± 1.1
Ash (%)	2.5 ± 0.4	1.0 ± 0.1
Total (%)	88.4 ± 1.2	79.8 ± 1.0

After lyophilization, the SA beads and CCNF/SA beads were obtained (Figure 3C). According to the SEM images, the surface of SA beads was smooth, while the CCNF/SA beads exhibited many wrinkles and rough surface, and the fiber-like CCNF aggregation was covered by SA (Figure 3D). In addition, the cross section of 50:1 beads exhibited more well-distributed pores around 100 μm (Figure 3E). From the point view of adsorption, the 50: 1 beads with coarse surface and porous inner structure were suitable to be used as dye adsorption materials.

Moreover, the chemical structure, thermo stability, and swelling properties of CCNF/SA beads were also investigated for the application of dye adsorption. As shown in Figure 4A, the broad peaks at 3340 and 2930 cm^{-1} belonged to the stretching vibration of O–H bond and C–H bond, respectively.[17] Compared with AM-R, the ether bonds peak of CCNF around 1030 cm^{-1} increased due to the introduction of cationic substituent group. The characteristic peak of CCNF at 1646 cm^{-1} belonged to the adsorbed water was covered by the -COONa peak of SA at 1601 cm^{-1}, and the peak of CCNF at 1441 cm^{-1} (-CH_3 of quaternary ammonium group) was also overlapped by the -COOH peak of SA at 1418 cm^{-1}.[12,18] In particular, the new peak of N element could be observed in X-ray photoelectron spectroscopy (XPS) spectrum of CCNF/SA beads (50:1) due to the presence of CCNF (Figure 7B). These phenomena indicated the chemical structure of CCNF and the cross-linked CCNF and SA in CCNF/SA composite beads. In addition, the thermal stability of CCNF/SA beads was obviously lower than that of CCNF, and higher than that of SA (Figures 4B and 4C). For CCNF/SA beads with different ratios of CCNF suspension and SA powder, the mass loss and degradation rate were similar. As reported, SA with poor thermal stability was not suitable to apply under high temperature conditions.[19] Therefore, CCNF/SA beads could be used as adsorption materials at room temperature.

Besides, the swelling ratio of CCNF/SA beads in water is also an important factor to evaluate water adsorption. A good dye adsorbent can selectively adsorb dyes, rather than water, which is helpful for the high-efficiency dye removal from wastewater treatment.[20] As shown in Figure 4D, the swelling ratio of SA beads was very high (84%), while the swelling ratio of all CCNF/SA beads was only around 26%, which indicated that the addition of CCNF decreased the water adsorption of the beads, and CCNF/SA beads were more suitable for dye adsorption than SA beads.

Adsorption properties of CCNF/SA beads

The effect of the mass ratio of CCNF suspension to SA powder, initial concentration of Congo red wastewater, and adsorption time and pH value of Congo red wastewater on adsorption properties of CCNF/SA beads were comprehensively investigated to optimize the adsorption conditions of Congo red. Firstly, the dye adsorption properties of CCNF/SA with different ratios (40:1, 50:1, and 60:1) were evaluated. The adsorption capacity at 25°C (Q_t) of 50:1 (CCNF: SA) beads was the largest at the initial concentration (C_0) of Congo red from 200 to 800 mg/L (Figure 5A). This result was because compared with the 40:1 and 60:1 beads, the better dispersibility of CCNF in the 50:1 beads, regular shape, and rough surface were beneficial to increase the contact area between beads and Congo red (Section 2.2). Furthermore, based on the N_2 adsorption desorption isotherms, the BET surface area of 50:1 beads was larger than other beads, confirming the higher adsorption capacity (Table 2). In addition, the lower pore volume of 40:1 and 60:1 beads indicated the blocked surface pores, thus decreasing the adsorption efficiency.[2] It was consistent with SEM cross-section image of the beads (Figure 3E). Therefore, the more suitable mass ratio of CCNF suspension to SA powder was 50:1, and the corresponding CCNF/SA beads (i.e., 50:1 beads) with better adsorption performance were used in the following work.

Moreover, the Q_t was increased with the increase of C_0 from 200 to 800 mg/L (Figure 5B). The Q_t could achieve the equilibrium at any concentration after 72 h, and the maximum Q_t was 518.4 mg/g at the C_0 of 800 mg/L. Simultaneously, the removal efficiency of Congo red was higher at low C_0 (200 mg/L), which could reach to 82% and 93% after 48 and 72 h of adsorption (Figure 5C), respectively. This phenomenon could also be observed in the insert image; the color of Congo red wastewater obviously became light and transparent.

In addition, pH value of Congo red wastewater had a remarkable impact on adsorption of Congo red. With the increase of pH value, the Q_t increased firstly and then declined; the maximum Q_t was at pH 5. As reported, when the pH was lower than 3, Congo red with the structure of o-quinone type internal salt exhibited blue color in solution. When the pH was larger than 5, Congo red with the sulfonate structure exhibited red color in solution.[21] Herein, CCNF with a large amount of positive charge could adsorb Congo red with negative charged sulfonate group under pH 5, leading to the high-efficient removal of Congo red. To sum up, CCNF/SA beads with the ratio of 50:1

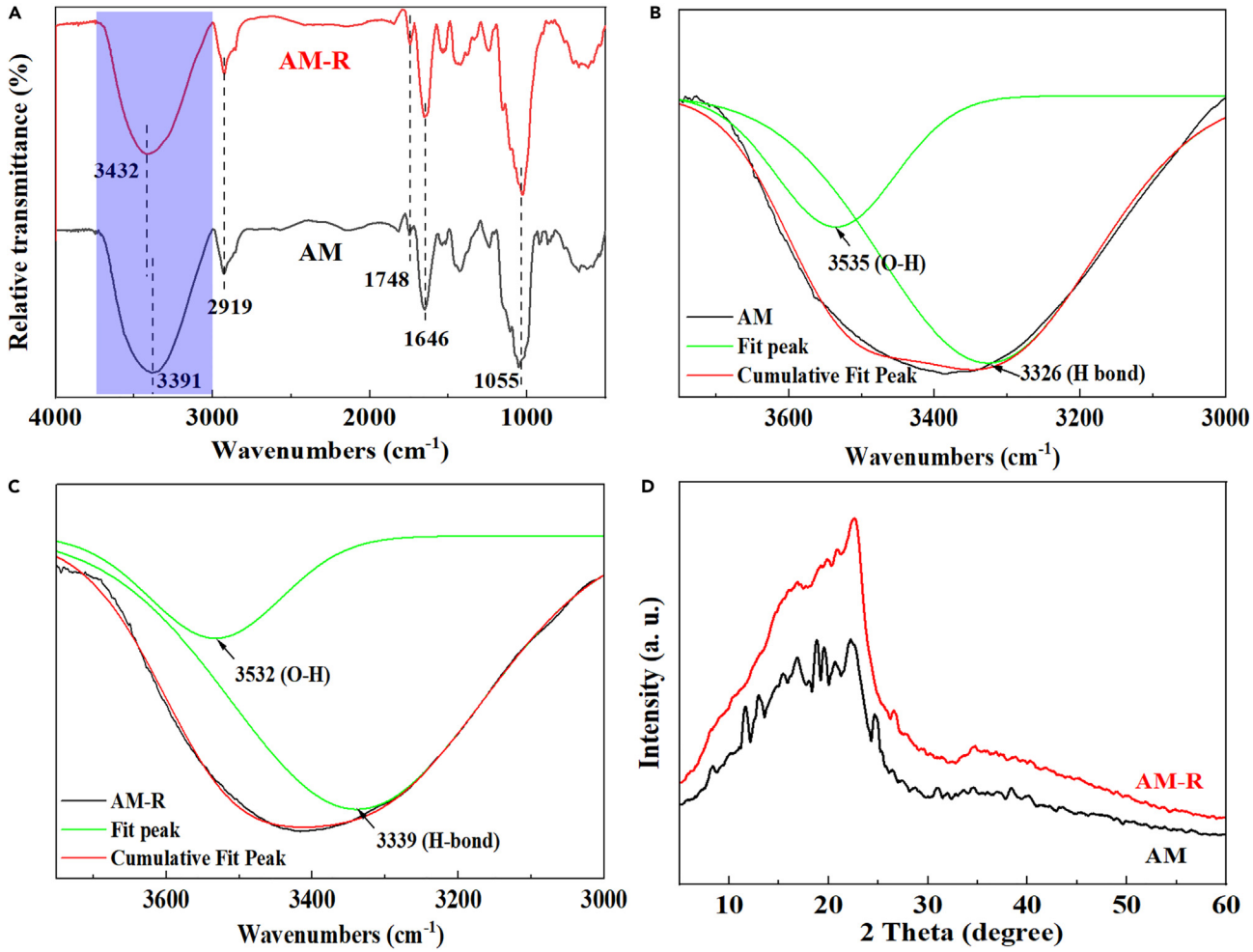

Figure 2. FTIR and XRD analysis of raw materials

(A) FTIR spectra of AM and AM-R; (B) Peak-differentiating and imitating of FTIR spectra of AM; (C) Peak-differentiating and imitating of FTIR spectra of AM-R; (D) XRD patterns of AM and AM-R.

exhibited an amazing adsorption performance of Congo red (the maximum Q_t of 518.4 mg/g and the removal efficiency of 93%) with adsorption time of 72 h at pH 5.

Adsorption model and kinetics

Langmuir and Freundlich adsorption isotherm models of CCNF/SA (50:1) beads were used to analyze the adsorption process. The fitting curves and parameters are shown in Figure 6A and Table 3, the correlation coefficients (R^2) of CCNF/SA beads for Langmuir and Freundlich models were 0.996 and 0.999, respectively, and the maximum adsorption capacity (Q_{max}) for Langmuir and Freundlich models (519.5 and

Table 2. Zeta potential of slurry and BET results of the corresponding beads

Samples	Zeta potential of slurry (mV)	Specific surface area (m^2/g)	Total pore volume (cm^3/g)
CCNF	54.8 ± 2.9	–	–
SA	–	4.936	0.091
40:1	50.6 ± 1.3	12.432	0.036
50:1	52.7 ± 7.1	12.799	0.056
60:1	53.2 ± 6.7	8.999	0.024

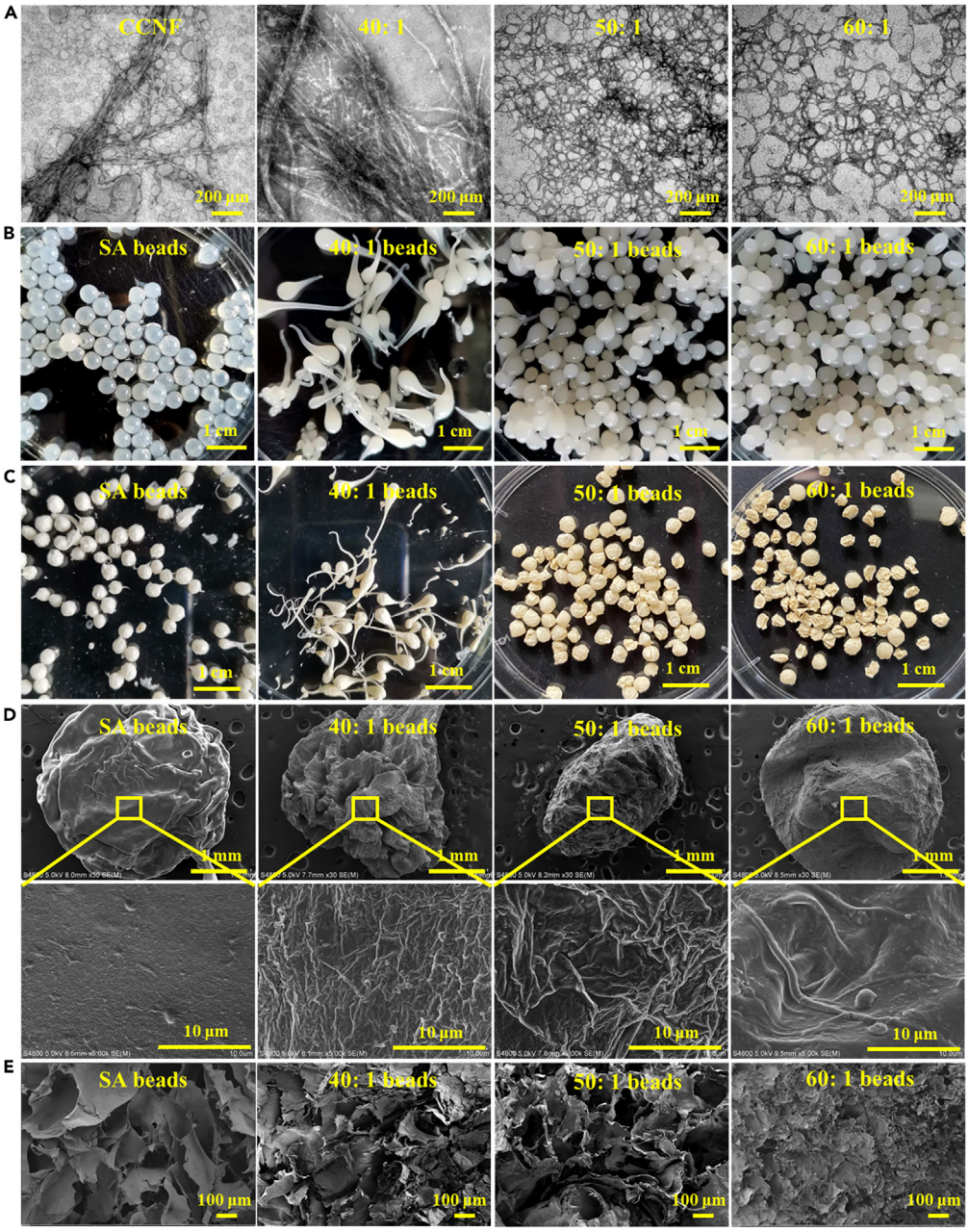

Figure 3. Morphological characterization

(A) TEM image of CCNF and CCNF/SA beads with different ratios; (B) Digital images of the wet beads; (C) Freeze-dried beads; Surface (D) and cross section (E) of the beads.

516.4 mg/g, respectively) was similar with the Q_e of experiment data (518.4 mg/g). These results indicated that the adsorption curves of CCNF/SA beads fitted perfectly for the two models, and the adsorption process easily proceeded.

Furthermore, the Q_e of CCNF/SA beads for Congo red was compared with other adsorbents, and it was higher than most reported cellulose-based adsorption materials (Figure 6B), such as cellulose/Fe_3O_4/activated carbon composite,[22] polyacrylamide grafted quaternized cellulose,[25] magnetic nanocellulose,[26] chitosan/cellulose hydrogel,[28] dialdehyde cellulose/chitosan beads,[30] β-cyclodextrin/cotton fibers,[34] polypyrrole modified nanocellulose,[36] graphene/cellulose aerogels,[37] bacterial cellulose/attapulgite composites,[38] etc. Although the Q_e of CCNF/SA beads was lower than that of porous $Fe(OH)_3$@Cellulose,[27] bacterial cellulose,[35] and cellulose nanofibril/carbon nanomaterial aerogels,[39] CCNF/SA beads had the advantages of simple preparation and relatively low-priced raw materials.

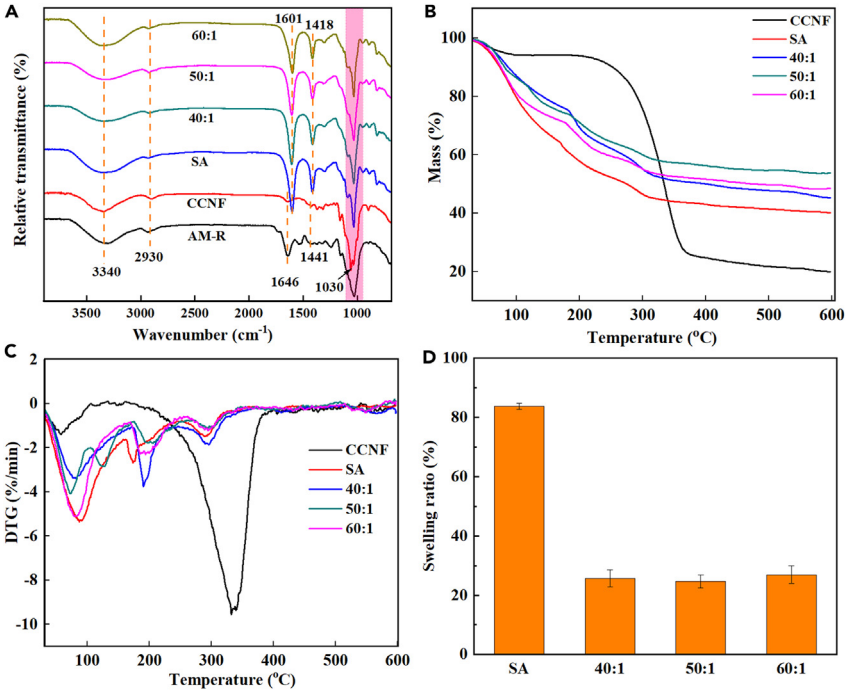

Figure 4. Characterization of CCNF/SA beads

(A) FTIR spectra of raw materials and CCNF/SA beads; (B, C) TG and DTG curves of SA and CCNF/SA beads; (D) Swelling ratio of SA and CCNF/SA beads.

In addition, the pseudo-first-order and pseudo-second-order adsorption models were used to investigate the adsorption kinetics of CCNF/SA beads for Congo red. The R^2 of pseudo-first-order curves of CCNF/SA beads was 0.909–0.956 at the concentrations from 200 to 800 mg/g, and the R^2 and K of pseudo-first-order model were higher compared to pseudo-second-order model (Figures 6C; Table 4). It indicated that the physical adsorption process was important and Congo red was easy to be adsorbed on CCNF/SA beads. Moreover, the adsorption curves of CCNF/SA beads fitted intra-particle diffusion model well, and the Q_{max} (model) was closer to the Q_e (experiment) at any concentration from 200 to 800 mg/L (Figures 6D; Table 4). In addition, these curves could be divided into two steps, Step I was mainly rapid adsorption for Congo red, and Step II was intra-particle diffusion process, which was the main rate-limiting step for the adsorption process of CCNF/SA beads.

Proposed adsorption mechanism

In order to investigate the adsorption mechanism of CCNF/SA beads, the FTIR and XPS characterizations of SA and 50:1 beads after Congo red adsorption (named as SA-CR and 50:1-CR, respectively) were conducted. As shown in Figure 7A, the new peak deduced to S=O stretching of Congo red at 1175 cm^{-1} could be observed in the spectra of SA-CR and 50:1-CR (SA and 50:1 beads after adsorption), confirming the adsorption of Congo red onto the beads. Due to the N=N stretching vibration peak of Congo red at 1582 cm^{-1},[43] the -COONa peak in 50:1 beads shifted from 1628 cm^{-1} to a lower wavenumber of 1597 cm^{-1}, and the -CH_3 peak of cationic group also shifted from 1441 to 1418 cm^{-1}, indicating the hydrogen bonds between functional groups of SA, CCNF, and Congo red.[2]

Furthermore, compared with SA and 50:1 beads before adsorption, the obvious peak of N element appeared at 400.1 eV in the wide-scan spectra of SA-CR and 50:1-CR beads (Figure 7B). It was mainly due to the introduced N element in Congo red. More importantly, the fit peak belonged to the quaternary ammonium group on CCNF around 399.6 eV decreased due to the electrostatic adsorption between quaternary ammonium group of CCNF and sulfonate group of Congo red, and there was a new fit peak at higher binding energy (402.1 eV) due to the formed -NH–C=O- group (Figures 7C and 7D). In addition, the peak of O1s was also shifted from 533.0 to 532.0 eV after adsorption (Figure 7E).[41,44] These results indicated the electrostatic adsorption involved in adsorption process.

Reusability study

Because the reusability is vital for the economic feasibility of the adsorbent, three adsorption-desorption cycles of 50:1 beads for Congo red removal were investigated. Because the adsorption capacity of CCNF/SA beads was strongly dependent on the pH value of Congo red solution (Figure 5D), NaOH solution was used as eluent to remove Congo red from CCNF/SA beads.[2] Results showed that the Congo red

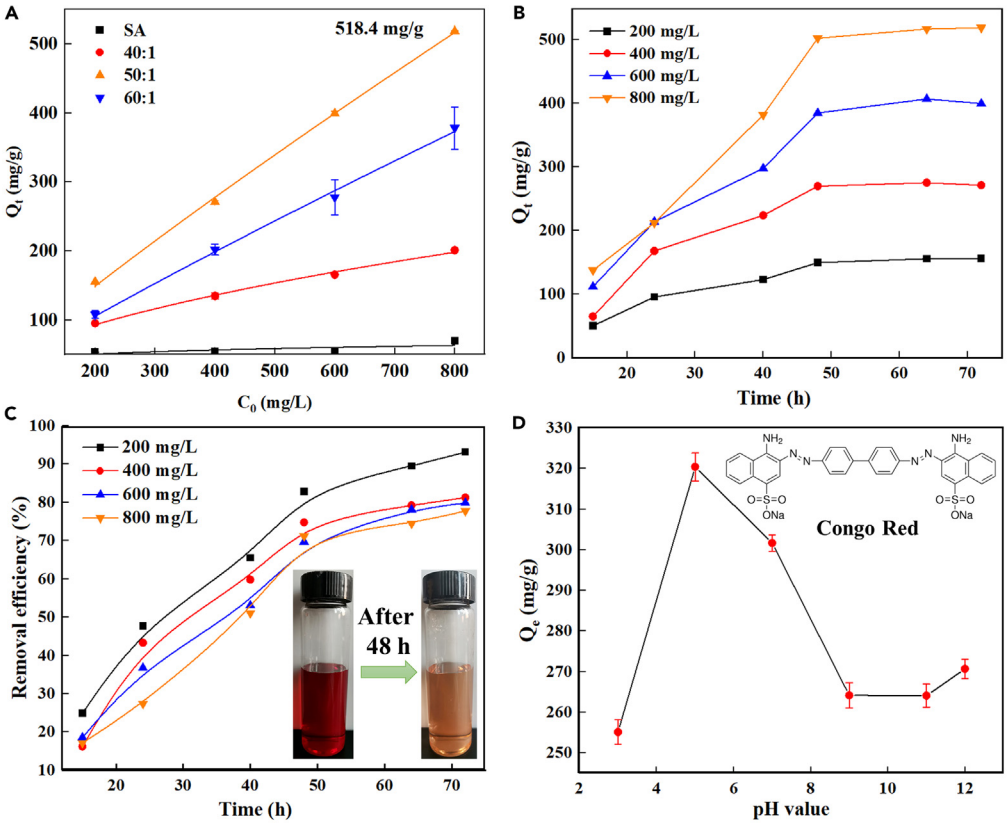

Figure 5. Adsorption capacity of CCNF/SA beads

(A) Adsorption capacity of SA and CCNF/SA beads at different concentrations of Congo red, pH 5, 72 h; (B) Adsorption capacity of 50:1 beads with different adsorption time, pH 5; (C) Removal efficiency of 50: 1 beads with different adsorption time, pH 5, the insert images is congo red solution before and after adsorption; (D) Adsorption capacity of 50:1 beads under different pH conditions, 600 mg/L.

removal efficiency of the beads slightly decreased with the increasing of cycles, but it was still higher than 70% after three cycles (Table 5). In addition, the desorption efficiency of Congo red in NaOH solution was 62.95% after three cycles in 1 h, suggesting that the 50:1 beads could be effectively regenerated and reused for the treatment of Congo red wastewater.

Conclusions

In this work, the CCNF/SA beads for adsorption Congo red were prepared using the AM-R and SA via physical crosslinking method. When the mass ratio of CCNF suspension (0.65 wt. %) to SA powder was 50: 1, the obtained CCNF/SA beads with relatively coarse surface, porous internal structure, and low swelling ratio were more suitable to be used as adsorption materials. The maximum adsorption capacity of the beads for Congo red was 518.4 mg/g at pH 5, and the corresponding removal efficiency of Congo red was 93% after 72 h. The amazing adsorption performance of CCNF/SA beads was superior to most reported cellulose-based adsorbents for Congo red. Moreover, the adsorption curve of CCNF/SA beads (50: 1) fitted perfectly for Langmuir and Freundlich adsorption models, and the adsorption process was in line with pseudo-first-order kinetics model, which indicated the physical adsorption process. Based on FTIR and XPS analysis, the proposed adsorption mechanism of the beads was mainly the hydrogen bonds and the electrostatic adsorption between quaternary ammonium group on CCNF and sulfonate groups on Congo red. In addition, the Congo red removal efficiency of the beads was higher than 70%, and the desorption efficiency in NaOH solution was 62.95% after three cycles, suggesting that the 50:1 beads could be effectively regenerated and reused for the treatment of Congo red wastewater. Therefore, the high efficiency and green CCNF/SA adsorbent is a good candidate for removal of Congo red and other anionic dyes.

Limitations of the study

This paper mainly focuses on the preparation of CCNF/SA composite beads and the application for Congo red removal; the removal of other anionic dyes needs to be further studied. In addition, more CNF-based advanced medical materials will be explored using Chinese herb solid residue as the starting material in future work.

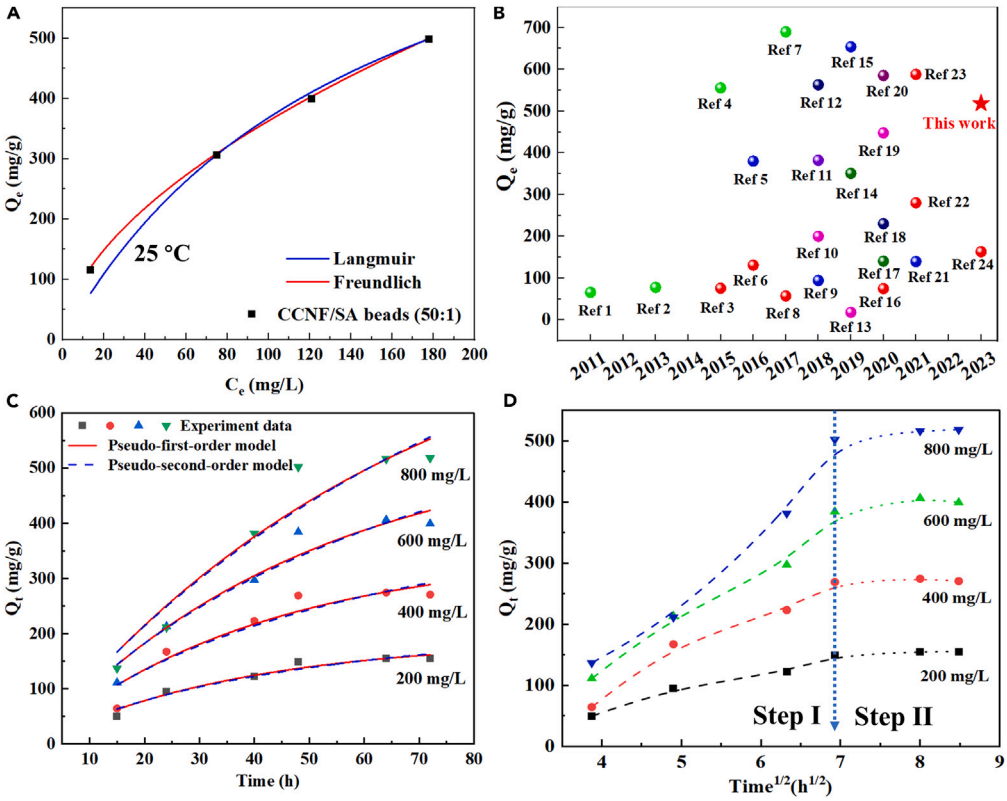

Figure 6. Equilibrium models and kinetic of adsorption

(A) Equilibrium adsorption isotherms of CCNF/SA beads, Langmuir and Freundlich models; (B) Comparison of the reported cellulose-based adsorption materials for Congo red removal; (C) Pseudo-first-order and Pseudo-second-order kinetics curves of CCNF/SA beads; (D) Intra-particle diffusion curves of CCNF/SA beads. Note: ref. 1, Cellulose/Fe_3O_4/activated carbon composite,[22] ref. 2, aminoethanethiol modified cellulose,[23] ref. 3, $CaCO_3$-decorated cellulose aerogel,[24] ref. 4, Amino-functionalized nanocrystalline cellulose,[9] ref. 5, Polyacrylamide grafted quaternized cellulose,[25] ref. 6, Magnetic nanocellulose,[26] ref. 7, Porous $Fe(OH)_3$@Cellulose,[27] ref. 8, Chitosan/cellulose hydrogel,[28] ref. 9, Polyaniline/carboxymethyl cellulose/TiO_2 nanocomposites,[29] ref. 10, Dialdehyde cellulose/chitosan beads,[30] ref. 11, Cellulose/chitosan composite,[31] ref. 12, Ionic liquid modified cellulose adsorbent,[32] ref. 13, Binary vinyl monomers modified cellulose,[33] ref. 14, β-cyclodextrin/cotton fibers,[34] ref. 15, Bacterial cellulose,[35] ref. 16, Polypyrrole modified nanocellulose,[36] ref. 17, Graphene/cellulose aerogels,[37] ref. 18, Bacterial cellulose/attapulgite composites,[38] ref. 19, Surfactant modified cellulose nanocrystals,[6] ref. 20, Cellulose nanofibril/carbon nanomaterial aerogels,[39] ref. 21, Cellulose beads loaded with graphene nanoplatelets,[40] ref. 22, Metal-organic framework/cellulose aerogel,[41] ref. 23, enzymatic hydrolysis residues,[21] ref. 24, $Mg(OH)_2$/cellulose paper fibers.[42]

STAR★METHODS

Detailed methods are provided in the online version of this paper and include the following:

- KEY RESOURCES TABLE
- RESOURCE AVAILABILITY
  - Lead contact
  - Material availability

Table 3. Langmuir and Freundlich model parameters of CCNF/SA beads for Congo red adsorption

	Langmuir model		Freundlich model		Experiment
Beads	R^2	Q_{max}	R^2	Q_{max}	Q_e (mg/g)
SA	0.319	57.7	0.665	63.2	69.5 ± 0.7
40:1	0.996	200.1	0.986	198.0	201.0 ± 2.0
50:1	0.996	519.5	0.999	516.4	518.4 ± 1.0
60:1	0.992	375.6	0.990	373.0	378.1 ± 30.6

The diameter of all beads is 0.2–0.4 cm.

Table 4. Parameters of pseudo-first-order, pseudo-second-order, and intra-particle diffusion models of CCNF/SA beads

Concentration	Pseudo-first-order			Pseudo-second-order			Intra-particle diffusion		Experiment
(mg/L)	K_1	R^2	Q_e	$K_2 \times 1000$	R^2	Q_e	R^2	Q_{max}	Q_e (mg/g)
200	0.027	0.956	188.9	0.070	0.946	279.4	0.972	158.0	155.2 ± 0.1
400	0.024	0.909	349.4	0.031	0.898	536.9	0.977	277.1	270.8 ± 1.9
600	0.020	0.951	555.6	0.015	0.945	880.8	0.957	414.0	399.2 ± 3.5
800	0.015	0.935	850.8	0.006	0.931	1446.1	0.926	542.6	518.4 ± 1.0

- Data and code availability
- METHOD DETAILS
  - Preparation of cationic cellulose nanofibrils (CCNF)
  - Preparation of CCNF/SA beads
  - Swelling of CCNF/SA beads
  - Adsorption capacity of CCNF/SA beads
  - Reuse of CCNF/SA beads
  - Characterization

ACKNOWLEDGMENTS

This research was financially supported by the National Natural Science Foundation of China (grant numbers U22A20423, 22208358), Shandong Energy Institute Research Foundation (No. SEI S202106), and Qingdao independent innovation major project (grant number 21-1-2-23-hz).

AUTHOR CONTRIBUTIONS

Conceptualization, B.L.; methodology, B.L.; investigation, M.W., Y.Z., X.F., and F.Y.; resources, Q.C. and B.L.; writing - original draft preparation, M.W.; writing - review and editing, Q.L. and B.L.; supervision and project administration, Q.C., Q.L. and B.L. All authors have read and agreed to the published version of the manuscript.

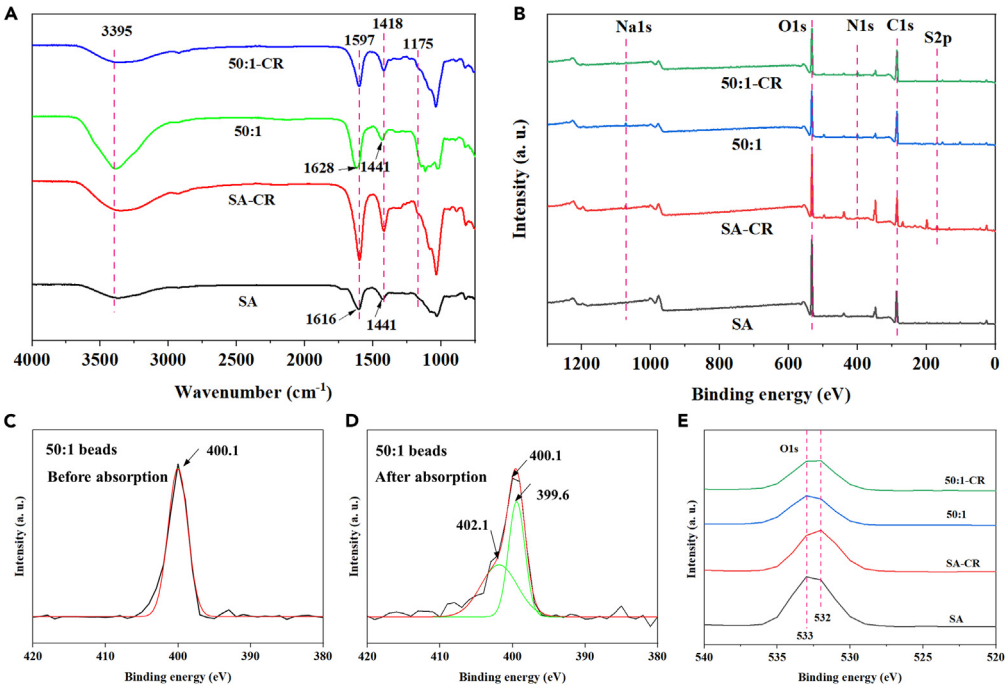

Figure 7. FTIR and XPS analysis of beads before and after adsorption

(A) FTIR spectra of SA and 50:1 beads before and after adsorption; (B) Wide-scan XPS spectra of SA and 50:1 beads before and after adsorption; N1s XPS analysis of 50:1 beads (C) and 50:1 beads after adsorption (D); (E) O1s XPS analysis of 50:1 beads.

Table 5. Recycling results of 50:1 beads

Cycle	Q_t (mg/g)	Removal efficiency (%)	Desorption efficiency (%)
1	470.32 ± 8.72	78.39 ± 1.45	87.61 ± 3.64
2	437.47 ± 14.21	72.91 ± 2.37	66.67 ± 2.39
3	428.94 ± 12.32	71.49 ± 2.05	62.95 ± 2.56

DECLARATION OF INTERESTS

The authors declare no conflict of interest.

INCLUSION AND DIVERSITY

We support inclusive, diverse, and equitable conduct of research.

Received: May 4, 2023
Revised: July 16, 2023
Accepted: August 28, 2023
Published: August 29, 2023

REFERENCES

1. Zhou, J., Cai, W., Yang, Z., Xia, Q., Chen, J., Fan, J., and Du, C. (2021). N,N-dimethylformamide assisted facile hydrothermal synthesis of boehmite microspheres for highly effective removal of Congo red from water. J. Colloid Interface Sci. *583*, 128–138. https://doi.org/10.1016/j.jcis.2020.09.004.
2. Liu, S., Ding, Y., Li, P., Diao, K., Tan, X., Lei, F., Zhan, Y., Li, Q., Huang, B., and Huang, Z. (2014). Adsorption of the anionic dye Congo red from aqueous solution onto natural zeolites modified with N,N-dimethyl dehydroabietylamine oxide. Chem. Eng. J. *248*, 135–144. https://doi.org/10.1016/j.cej.2014.03.026.
3. Yu, C.-X., Chen, J., Zhang, Y., Song, W.-B., Li, X.-Q., Chen, F.-J., Zhang, Y.-J., Liu, D., and Liu, L.-L. (2021). Highly efficient and selective removal of anionic dyes from aqueous solution by using a protonated metal-organic framework. J. Alloys Compd. *853*, 157383. https://doi.org/10.1016/j.jallcom.2020.157383.
4. Zheng, Y., Cheng, B., Fan, J., Yu, J., and Ho, W. (2021). Review on nickel-based adsorption materials for Congo red. J. Hazard. Mater. *403*, 123559. https://doi.org/10.1016/j.jhazmat.2020.123559.
5. Okesola, B.O., and Smith, D.K. (2016). Applying low-molecular weight supramolecular gelators in an environmental setting - self-assembled gels as smart materials for pollutant removal. Chem. Soc. Rev. *45*, 4226–4251. https://doi.org/10.1039/c6cs00124f.
6. Ranjbar, D., Raeiszadeh, M., Lewis, L., MacLachlan, M.J., and Hatzikiriakos, S.G. (2020). Adsorptive removal of Congo red by surfactant modified cellulose nanocrystals: a kinetic, equilibrium, and mechanistic investigation. Cellulose *27*, 3211–3232. https://doi.org/10.1007/s10570-020-03021-z.
7. Şenol, Z.M., Gürsoy, N., Şimşek, S., Özer, A., and Karakuş, N. (2020). Removal of food dyes from aqueous solution by chitosan-vermiculite beads. Int. J. Biol. Macromol. *148*, 635–646. https://doi.org/10.1016/j.ijbiomac.2020.01.166.
8. Huo, M.X., Jin, Y.L., Sun, Z.F., Ren, F., Pei, L., and Ren, P.G. (2021). Facile synthesis of chitosan-based acid-resistant composite films for efficient selective adsorption properties towards anionic dyes. Carbohydr. Polym. *254*, 117473. https://doi.org/10.1016/j.carbpol.2020.117473.
9. Jin, L., Li, W., Xu, Q., and Sun, Q. (2015). Amino-functionalized nanocrystalline cellulose as an adsorbent for anionic dyes. Cellulose *22*, 2443–2456. https://doi.org/10.1007/s10570-015-0649-4.
10. Zeng, P., Li, J., Chen, Y., and Zhang, L. (2019). The structures and biological functions of polysaccharides from traditional Chinese herbs. Prog. Mol. Biol. Transl. Sci. *163*, 423–444. https://doi.org/10.1016/bs.pmbts.2019.03.003.
11. Jiang, T., Feng, X., Xu, R., Dong, S., Wu, M., Zheng, X., Lu, W., and Li, B. (2021). A handy skin wound dressing prepared by alginate and cationic nanofibrillated cellulose derived from solid residues of herbs. Bioresources *16*, 5926–5946.
12. Zhao, X., Wang, X., and Lou, T. (2021). Preparation of fibrous chitosan/sodium alginate composite foams for the adsorption of cationic and anionic dyes. J. Hazard. Mater. *403*, 124054. https://doi.org/10.1016/j.jhazmat.2020.124054.
13. Tang, S., Yang, J., Lin, L., Peng, K., Chen, Y., Jin, S., and Yao, W. (2020). Construction of physically crosslinked chitosan/sodium alginate/calcium ion double-network hydrogel and its application to heavy metal ions removal. Chem. Eng. J. *393*, 124728. https://doi.org/10.1016/j.cej.2020.124728.
14. Wang, Q., Du, H., Zhang, F., Zhang, Y., Wu, M., Yu, G., Liu, C., Li, B., and Peng, H. (2018). Flexible cellulose nanopaper with high wet tensile strength, high toughness and tunable ultraviolet blocking ability fabricated from tobacco stalk via a sustainable method. J Mater. Chem. A *6*, 13021–13030. https://doi.org/10.1039/c8ta01986j.
15. Wu, M., Sukyai, P., Lv, D., Zhang, F., Wang, P., Liu, C., and Li, B. (2020). Water and humidity-induced shape memory cellulose nanopaper with quick response, excellent wet strength and folding resistance. Chem. Eng. J. *392*, 123673. https://doi.org/10.1016/j.cej.2019.123673.
16. Huang, Z., Liu, C., Feng, X., Wu, M., Tang, Y., and Li, B. (2020). Effect of regeneration solvent on the characteristics of regenerated cellulose from lithium bromide trihydrate molten salt. Cellulose *27*, 9243–9256. https://doi.org/10.1007/s10570-020-03440-y.
17. Wu, M., Yu, G., Chen, W., Dong, S., Wang, Y., Liu, C., and Li, B. (2022). A pulp foam with highly improved physical strength, fire-resistance and antibiosis by incorporation of chitosan and CPAM. Carbohydr. Polym. *278*, 118963. https://doi.org/10.1016/j.carbpol.2021.118963.
18. Gao, Y., Li, Q., Shi, Y., and Cha, R. (2016). Preparation and application of cationic modified cellulose fibrils as a papermaking additive. Int. J. Poly. Sci. *2016*, 1–8. https://doi.org/10.1155/2016/6978434.
19. Gao, C., Liu, M., Chen, J., and Zhang, X. (2009). Preparation and controlled degradation of oxidized sodium alginate hydrogel. Polym. Degrad. Stab. *94*, 1405–1410. https://doi.org/10.1016/j.polymdegradstab.2009.05.011.
20. Sharma, R.K., and Kumar, R. (2019). Functionalized cellulose with hydroxyethyl methacrylate and glycidyl methacrylate for metal ions and dye adsorption applications. Int. J. Biol. Macromol. *134*, 704–721. https://doi.org/10.1016/j.ijbiomac.2019.05.059.
21. Xu, R., Du, H., Liu, C., Liu, H., Wu, M., Zhang, X., Si, C., and Li, B. (2021). An efficient and magnetic adsorbent prepared in a dry process with enzymatic hydrolysis residues for wastewater treatment. J. Clean. Prod. *313*, 127834. https://doi.org/10.1016/j.jclepro.2021.127834.
22. Zhu, H.Y., Fu, Y.Q., Jiang, R., Jiang, J.H., Xiao, L., Zeng, G.M., Zhao, S.L., and Wang, Y. (2011). Adsorption removal of congo red onto magnetic cellulose/Fe3O4/activated carbon composite: Equilibrium, kinetic and thermodynamic studies. Chem. Eng. J. *173*, 494–502. https://doi.org/10.1016/j.cej.2011.08.020.

23. Silva, L.S., Lima, L.C.B., Silva, F.C., Matos, J.M.E., Santos, M.R.M.C., Santos Júnior, L.S., Sousa, K.S., and da Silva Filho, E.C. (2013). Dye anionic sorption in aqueous solution onto a cellulose surface chemically modified with aminoethanethiol. Chem. Eng. J. *218*, 89–98. https://doi.org/10.1016/j.cej.2012.11.118.
24. Chong, K.Y., Chia, C.H., Zakaria, S., Sajab, M.S., Chook, S.W., and Khiew, P.S. (2015). $CaCO_3$-decorated cellulose aerogel for removal of Congo Red from aqueous solution. Cellulose *22*, 2683–2691. https://doi.org/10.1007/s10570-015-0675-2.
25. Wang, Y., Zhao, L., Peng, H., Wu, J., Liu, Z., and Guo, X. (2016). Removal of anionic dyes from aqueous solutions by cellulose-based adsorbents: Equilibrium, kinetics, and thermodynamics. J. Chem. Eng. Data *61*, 3266–3276. https://doi.org/10.1021/acs.jced.6b00340.
26. Beyki, M.H., Bayat, M., and Shemirani, F. (2016). Fabrication of core-shell structured magnetic nanocellulose base polymeric ionic liquid for effective biosorption of Congo red dye. Bioresour. Technol. *218*, 326–334. https://doi.org/10.1016/j.biortech.2016.06.069.
27. Zhao, J., Lu, Z., He, X., Zhang, X., Li, Q., Xia, T., Zhang, W., and Lu, C. (2017). Fabrication and characterization of highly porous $Fe(OH)_3$@cellulose hybrid fibers for effective removal of Congo red from contaminated water. ACS Sustain. Chem. Eng. *5*, 7723–7732. https://doi.org/10.1021/acssuschemeng.7b01175.
28. Tu, H., Yu, Y., Chen, J., Shi, X., Zhou, J., Deng, H., and Du, Y. (2017). Highly cost-effective and high-strength hydrogels as dye adsorbents from natural polymers: chitosan and cellulose. Polym. Chem. *8*, 2913–2921. https://doi.org/10.1039/c7py00223h.
29. Tanzifi, M., Tavakkoli Yaraki, M., Karami, M., Karimi, S., Dehghani Kiadehi, A., Karimipour, K., and Wang, S. (2018). Modelling of dye adsorption from aqueous solution on polyaniline/carboxymethyl cellulose/TiO_2 nanocomposites. J. Colloid Interface Sci. *519*, 154–173. https://doi.org/10.1016/j.jcis.2018.02.059.
30. Ruan, C.Q., Strømme, M., and Lindh, J. (2018). Preparation of porous 2,3-dialdehyde cellulose beads crosslinked with chitosan and their application in adsorption of Congo red dye. Carbohydr. Polym. *181*, 200–207. https://doi.org/10.1016/j.carbpol.2017.10.072.
31. Wang, Y., Wang, H., Peng, H., Wang, Z., Wu, J., and Liu, Z. (2018). Dye adsorption from aqueous solution by cellulose/chitosan composite: equilibrium, kinetics, and thermodynamics. Fiber. Polym. *19*, 340–349. https://doi.org/10.1007/s12221-018-7520-9.
32. Zhang, S.-F., Yang, M.-X., Qian, L.-W., Hou, C., Tang, R.-H., Yang, J.-F., and Wang, X.-C. (2018). Design and preparation of a cellulose-based adsorbent modified by imidazolium ionic liquid functional groups and their studies on anionic dye adsorption. Cellulose *25*, 3557–3569. https://doi.org/10.1007/s10570-018-1815-2.
33. Sharma, R.K., Kumar, R., and Singh, A.P. (2019). Metal ions and organic dyes sorption applications of cellulose grafted with binary vinyl monomers. Sep. Purif. Technol. *209*, 684–697. https://doi.org/10.1016/j.seppur.2018.09.011.
34. Yue, X., Huang, J., Jiang, F., Lin, H., and Chen, Y. (2019). Synthesis and characterization of cellulose-based adsorbent for removal of anionic and cationic dyes. J. Eng. Fiber Fabr. *14*, 1–10. https://doi.org/10.1177/1558925019828194.
35. Hu, Y., Liu, F., Sun, Y., Xu, X., Chen, X., Pan, B., Sun, D., and Qian, J. (2019). Bacterial cellulose derived paper-like purifier with multifunctionality for water decontamination. Chem. Eng. J. *371*, 730–737. https://doi.org/10.1016/j.cej.2019.04.091.
36. Shahnaz, T., S, M.M.F., Vc, P., and Narayanasamy, S. (2020). Surface modification of nanocellulose using polypyrrole for the adsorptive removal of Congo red dye and chromium in binary mixture. Int. J. Biol. Macromol. *151*, 322–332. https://doi.org/10.1016/j.ijbiomac.2020.02.181.
37. Feng, C., Ren, P., Li, Z., Tan, W., Zhang, H., Jin, Y., and Ren, F. (2020). Graphene/waste-newspaper cellulose composite aerogels with selective adsorption of organic dyes: preparation, characterization, and adsorption mechanism. New J. Chem. *44*, 2256–2267. https://doi.org/10.1039/c9nj05346h.
38. Chen, X., Cui, J., Xu, X., Sun, B., Zhang, L., Dong, W., Chen, C., and Sun, D. (2020). Bacterial cellulose/attapulgite magnetic composites as an efficient adsorbent for heavy metal ions and dye treatment. Carbohydr. Polym. *229*, 115512. https://doi.org/10.1016/j.carbpol.2019.115512.
39. Yu, Z., Hu, C., Dichiara, A.B., Jiang, W., and Gu, J. (2020). Cellulose nanofibril/carbon nanomaterial hybrid aerogels for adsorption removal of cationic and anionic organic dyes. Nanomaterials *10*, 169. https://doi.org/10.3390/nano10010169.
40. González-López, M.E., Laureano-Anzaldo, C.M., Pérez-Fonseca, A.A., Gómez, C., and Robledo-Ortíz, J.R. (2021). Congo red adsorption with cellulose-graphene nanoplatelets beads by differential column batch reactor. J. Environ. Chem. Eng. *9*, 105029. https://doi.org/10.1016/j.jece.2021.105029.
41. Huang, C., Cai, B., Zhang, L., Zhang, C., and Pan, H. (2021). Preparation of iron-based metal-organic framework @cellulose aerogel by in situ growth method and its application to dye adsorption. J. Solid State Chem. *297*, 122030. https://doi.org/10.1016/j.jssc.2021.122030.
42. Jiang, D., Chen, H., Xie, H., Cheng, K., Li, L., Xie, K., and Wang, Y. (2023). Fe, N, S co-doped cellulose paper carbon fibers as an air-cathode catalyst for microbial fuel cells. Environ. Res. *221*, 115308. https://doi.org/10.1016/j.envres.2023.115308.
43. Kim, U.J., Kimura, S., and Wada, M. (2019). Highly enhanced adsorption of Congo red onto dialdehyde cellulose-crosslinked cellulose-chitosan foam. Carbohydr. Polym. *214*, 294–302. https://doi.org/10.1016/j.carbpol.2019.03.058.
44. Wang, F., Zhang, L., Wang, Y., Liu, X., Rohani, S., and Lu, J. (2017). Fe_3O_4 @SiO_2 @CS-TETA functionalized graphene oxide for the adsorption of methylene blue (MB) and Cu(II). Appl. Surf. Sci. *420*, 970–981. https://doi.org/10.1016/j.apsusc.2017.05.179.
45. Sluiter, J.B., Ruiz, R.O., Scarlata, C.J., Sluiter, A.D., and Templeton, D.W. (2010). Compositional analysis of lignocellulosic feedstocks. Review and description of methods. J. Agric. Food Chem. *58*, 9043–9053. https://doi.org/10.1021/jf1008023.

STAR★METHODS

KEY RESOURCES TABLE

REAGENT or RESOURCE	SOURCE	IDENTIFIER
Chemicals, peptides, and recombinant proteins		
Astragalus Membranaceus root	Juyaotang	P1912013
Sodium alginate	Sinopharm	CAS: 9005-38-3, viscosity ≥0.02 Pa s
2, 3-glycidyl trimethyl ammonium chloride	Sinopharm	CAS: 3033-77-0, ≥95.0%
Calcium chloride anhydrous	Sinopharm	CAS: 10043-52-4, ≥96.0%
NaOH	Sinopharm	CAS: 1310-73-2, ≥96.0%
Congo red	BASF	CAS: 573-58-0, ≥98.0%

RESOURCE AVAILABILITY

Lead contact

Further information and requests for resources and reagents should be directed to and will be fulfilled by the lead contact, Bin Li (libin@qibebt.ac.cn).

Material availability

The Astragalus Membranaceus root and the obtained CCNF/SA beads in this study can be made available on request.

Data and code availability

- All data reported in this paper will be shared by the lead contact upon request.
- This paper does not report original code.
- Any additional information required to reanalyze the data reported in this paper is available from the lead contact upon request.

METHOD DETAILS

Preparation of cationic cellulose nanofibrils (CCNF)

Firstly, 10 g AM was boiled at 100°C together with 1000 mL deionized water for 30 min, and then followed by solid-liquid separation. The obtained AM solid was further boiled with 1000 mL fresh deionized water through the same procedure. After that, the obtained AM solid residue was air-dried, ball-milled, and screened, to get 30–80 mesh AM residues (AM-R) containing cellulose, hemicellulose and lignin.

After that, AM-R was subjected to alkalization and etherification to produce CCNF. Specifically, 5 g AM-R was immersed in deionized water with a consistency of 10 wt. % at room temperature (20°C) for 12 h, and then 10 g NaOH was added in the mixture under mildly magnetic stirring at room temperature for 3 h to alkalify. After alkalization, the AM-R were washed with deionized water thoroughly. Subsequently, the collected AM-R were mixed with NaOH (5 g), 2, 3-glycidyl trimethyl ammonium chloride (10 g) and alcohol (80 mL) in a plastic sealing bag for etherification. The reaction was sustained for 15 h at 50°C and then the solid residues were rinsed with deionized water until the pH was neutral. Then, the solid residues were dispersed in deionized water and the suspension was homogenized by a high-pressure homogenizer (ATH Engineering, Ltd., Suzhou, China) for 30 min at 700 bar to obtain the CCNF suspension with the consistency of 0.65 wt. %.

Preparation of CCNF/SA beads

CCNF/SA beads were prepared via ionic gelation method. Firstly, different mass ratios (40:1, 50:1 and 60:1) of CCNF suspension with the concentration of 0.65 wt. % to SA powder were vigorously stirred at room temperature for 2 h to form homogeneous slurry. Then, the slurry was added in $CaCl_2$ solution (200 mL, 0.25 M) dropwise at room temperature. The control sample (SA beads) was prepared by adding SA solution (5 wt. %) in $CaCl_2$ solution. All beads were collected from $CaCl_2$ solution and then freeze-dried. The obtained beads were labeled as CCNF/SA (40:1, 50:1, 60:1) beads and SA beads.

Swelling of CCNF/SA beads

Freeze-dried CCNF/SA and SA beads were first pre-weighted as W_0, and then immersed in deionized water at 25°C for 24 h. After that, the hydrated beads were carefully wiped with filter paper to remove free water on the surface, and then weighted as W_1, the swelling ratio was calculated by the following formula 1.

$$Swelling\ ratio = \frac{W_1 - W_0}{W_0} \times 100\% \quad \text{(Equation 1)}$$

Adsorption capacity of CCNF/SA beads

Specifically, 30 mg lyophilized CCNF/SA beads or SA beads were added in a beaker containing 20 mL Congo red solution at different concentrations (200, 400, 600 and 800 mg/L), and the beakers were placed in a water bath at 25°C for a certain time. To evaluate the effect of the pH on adsorption capacity, 50 mg CCNF/SA beads (50:1) was agitated with 20 mL Congo red solution with different pH value at 25°C for 72 h. The pH value of Congo red solution with a concentration of 600 mg/L was adjusted to 3, 5, 7, 9, 11 and 12 using 1 M HCl or 1 M NaOH solution. After adsorption, the beads were removed from the solution, and the concentration of Congo red in the supernatant was measured by a UV-vis spectrophotometer (YOKE Instrument, UV752, China) at 495 nm. All adsorption tests were repeated at least three times.

The adsorption amount of the CCNF/SA beads for Congo red at time t and equilibrium, named as Q_t and Q_e (mg/g), respectively, were calculated according to the following Equations 2 and 3. The removal efficiency (%) of Congo red was calculated based on the formula (4).

$$Q_t = \frac{(C_0 - C_t) * V}{m} \quad \text{(Equation 2)}$$

$$Q_e = \frac{(C_0 - C_e) * V}{m} \quad \text{(Equation 3)}$$

$$Removal\ efficiency\ (\%) = \frac{(C_0 - C_e) * V}{C_0 * V} * 100\% \quad \text{(Equation 4)}$$

Where, C_0 (mg/L) is the initial concentration of Congo red, C_e and C_t (mg/L) are the equilibrium concentration and concentration at time t (h), V (L) is the volume of the adsorbate solution, and m (g) is the mass of the beads.

Langmuir and Freundlich adsorption isotherms were described by the formulas (5) and (6), the pseudo-first-order and pseudo-second-order adsorption models for analyzing the adsorption kinetics were described by the formulas (7) and (8), and intra-particle diffusion model was expressed as the formula (9).

$$Q_e = \frac{Q_{max} \times b \times C_e}{1 + b \times C_e} \quad \text{(Equation 5)}$$

$$Q_e = K_F \times C_e^{1/n} \quad \text{(Equation 6)}$$

$$Q_t = Q_e \times \left(1 - e^{k_1 t}\right) \quad \text{(Equation 7)}$$

$$Q_t = \frac{Q_e^2 k_2 t}{1 + Q_e k_2 t} \quad \text{(Equation 8)}$$

$$Q_t = k_3 t^{1/2} + C \quad \text{(Equation 9)}$$

Where, Q_{max} is theoretical maximum adsorption capacity (mg/g), b is Langmuir constant, C_e and C_t (mg/L) are the equilibrium adsorption concentration and concentration at time t, K_F (mg/g) and n are the Freundlich constants related to adsorption capacity and heterogeneity factor, respectively, and k_1 and k_2 are the kinetics rate constants of the pseudo-first-order and pseudo-second-order models, respectively. k_3 is the intra-particle diffusion rate constant and C (mg/g) is the thickness of the boundary layer.

Reuse of CCNF/SA beads

After adsorption at 25°C for 72 h, the Congo red-loaded CCNF/SA beads (50:1) were filtered from the Congo red solution (600 mg/L), and then immersed in 50 mL of 0.1 mol/L NaOH solution. The solution was softly shaken for 1 h at 25°C for Congo red desorption. Subsquently, 50:1 beads were softly filtered and washed for three times with deionized water, and then reused for next cycle. The adsorption-desorption process was repteated for three times to evaluate the reuse performance of CCNF/SA beads. The removal efficiency of Congo red and desorption efficiency were caculated based on formula (4).

Characterization

The chemical compositions of AM and AM-R were measured according to the National Renewable Energy Laboratory procedure.[45] The Zeta potential of CCNF and CCNF/SA slurry was tested with a Zeta potential instrument (Brookhaven instrument, NanoBrook 90 Plus, USA). Before testing, the CCNF samples were diluted to 0.01 wt. % and then ultrasonically treated (45 kHz, 180 W) for 15 min. The degree of substitution (DS) of quaternary ammonium groups was determined using an element analyzer (Vario EL III, Germany) by the nitrogen content (N%) of CCNF based on the formula (10).

$$DS = \frac{162 \times N\%}{14 - 151.5 \times N\%} \quad \text{(Equation 10)}$$

Where, 162 is the molecular weight of anhydroglucose unit, and 151.5 is the molecular weight of the substituted group.

CCNF and CCNF/SA slurry were taken on a transmission electron microscope (TEM, Hitachi H-7600, Japan) with an accelerating voltage of 100 kV. Before measurement, the diluted CCNF and CCNF/SA solution with a consistency of 0.01 wt. % were suffered to ultrasonically dispersion (45 kHz, 180 W) for 30 min. Then, a droplet of slurry samples was deposited on a carbon-supported copper grid and dried at room temperature. Subsequently, the dry sample was dyed with uranyl acetate (20 μL, 2 wt. %) to enhance the contrast of images. The morphology of CCNF/SA and SA beads was characterized with a scanning electron microscope (SEM, Hitachi S-4800, Japan) at 5.0 kV. All samples were coated with gold under vacuum before observation. The Fourier transform infrared spectroscopy (FTIR) spectra of dried AM-R, CCNF, SA, CCNF/SA power were measured using a spectrometer (Thermo Fisher, Nicolet 6700, USA) with a wavenumber range of 4000-750 cm^{-1}, and KBr pellet method was carried out for sample preparation before test. The X-ray Diffraction patterns of AM and AM-R were recorded using an X-ray diffractometer (Bruker Discover D8, Germany). The Brunner-Emmet-Teller (BET) specific surface areas and pore volume of SA and CCNF/SA beads were determined by N_2 adsorption-desorption method using an automatic surface analyzer (Quantachrome instruments, autosorb iQ, USA). The thermal stability of CCNF, SA and CCNF/SA samples were analyzed by a thermal gravimetric instrument (TG, NETZSCH STA449F5 jupiter, Germany). The temperature ascended from 30°C to 600 °C at a heating rate of 10°C/min under nitrogen (25 mL/min). The Attenuated total reflection-Fourier transform infrared spectroscopy (ATR-FTIR) spectra of dried SA, 50:1 beads before and after adsorption (adsorbent amount 1.5 mg/mL Congo red solution, Congo red concentration 600 mg/L, 24 h) were carried out with a range of 4000-750 cm^{-1}. X-ray photoelectron spectroscopy (XPS) spectra of the 50:1 beads before and after adsorption were collected using a spectrometer (Thermo fisher, ESCALAB 250Xi, USA) at an analyzer pass energy of 100 eV.